Far-infrared phonon absorption in InSb†

E. S. Koteles and W. R. Datars
Department of Physics, McMaster University, Hamilton, Ontario, Canada

G. Dolling
Chalk River Nuclear Laboratories, Atomic Energy of Canada Limited, Chalk River, Ontario, Canada

(Received 4 September 1973)

Far-infrared absorption due to single-phonon and two-phonon processes was investigated in undoped InSb using a high-resolution Fourier-transform spectrometer. Single-phonon absorption by both transverse- and longitudinal-optical modes at the Brillouin-zone center was observed. Two-phonon absorption spectra correlated well with two-phonon density-of-states curves calculated using parameters derived from inelastic-neutron-scattering experiments. Brillouin-zone locations of critical points that gave rise to prominent features on the two-phonon density-of-states curve were identified by investigating phonon frequency contours on symmetry planes. Critical points at (0.6, 0, 0), X, and L for phonon combinations involving transverse modes and on the (111) boundary plane of the Brillouin zone for combinations containing the longitudinal-acoustical phonon gave rise to almost all the prominent features observed on the two-phonon absorption spectra. Derived frequencies for phonon modes at (0.6, 0, 0), X, and L agreed well with values determined directly from inelastic-neutron-scattering experiments. Although strong features, arising from 2TA overtones at X and L, appear in the calculated spectrum, no absorption corresponding to these features was observed.

I. INTRODUCTION

Far-infrared multiphonon-absorption spectroscopy offers the possibility of determining very accurately the energies of phonons at certain locations in the Brillouin zone. This necessitates the unambiguous identification of spectral features with critical points of phonon-combination branches at points in the Brillouin zone. In recent years, much work has been done to interpret such spectra in a variety of semiconductors.[1] Essentially, such investigations assumed that the frequency dependence of the photon-phonon coupling mechanism was slow compared with the rapid changes due to discontinuities in the multiphonon density-of-states curves. In this way, all of the features observed in the absorption spectra were attributed to van Hove singularities[2] in the density-of-states curves at critical points on the phonon-dispersion curves. Generally, it was further tacitly assumed that only critical points at high-symmetry points in the Brillouin zone resulted in prominent features on the density-of-states curves.

The multiphonon spectra of InSb, a III-V compound semiconductor with the zinc-blende structure, has been analyzed in this manner by Johnson,[1] Fray *et al.*[3] and Stierwalt.[4] (The last investigation employed far-infrared emission, which can be thought of, in simple terms, as the inverse of an absorption experiment.) The energies that were determined for phonons at high-symmetry points in these experiments were not entirely in accord with each other and, in some cases, disagreed with values measured in a recent inelastic-neutron-scattering experiment.[5]

In this paper, a more thorough analysis of far-infrared absorption in InSb, observed with a far-infrared Michelson interferometer, was undertaken in an attempt to resolve these difficulties. The parameters derived by Price *et al.*[5] from a fit of a shell model to their experimental data were utilized in calculations of two-phonon density-of-states curves. The general agreement between these calculated curves and our experimental high-resolution absorption curves made possible a detailed critical-point analysis employing phonon-energy contours. Calculated phonon energies were used to determine constant-energy contours on the major symmetry planes of the Brillouin zone. The positions of critical points giving rise to prominent features on the density-of-states curves were located with accuracy by locating areas where the phonon energy was stable or a weak function of wave vector. The majority of the observed features of the absorption spectra were correlated with similar ones on the calculated two-phonon density-of-states curves which, in turn, were traced to critical points. These points were not necessarily symmetry points. All of the remaining prominent features could be assigned to critical points of combinations of the transverse-optical mode using experimental two-phonon dispersion curves.

The far-infrared radiation field simultaneously interacts with two phonons via second-order dipole moments and/or third-order terms in the lattice potential.[6] The absolute magnitudes of these coupling mechanisms have not been calculated explicitly for semiconductors but it has been suggested that they are of equal importance in compound

semiconductors.[7] The interpretation of multiphonon spectra usually commences with the assumption that the frequency dependence of the coupling strength is smooth and slow. Thus features, such as peaks and discontinuities, present in the observed spectra are not considered to be consequences of this term but rather are attributed to features on the multiphonon density-of-states curves. In the case of InSb this appears to be a good preliminary assumption in the analysis of such spectra. However, direct evidence of the importance of the coupling mechanism is given by the absence of certain peaks in the observed spectra that are predicted by the calculated density of states.

II. EXPERIMENTAL METHOD

The Consolidated Mining and Smelting Co. of Canada provided the InSb samples studied in these experiments. The n-type single-crystal material was undoped and possessed a nominal electron mobility of 6×10^5 cm^2 V^{-1} sec^{-1} and a nominal carrier concentration of 10^{14} cm^{-3} at liquid-nitrogen temperatures. Samples were cut into the required shape with a spark cutter and then lapped with various grades of sandpaper until the proper thickness and wedging were achieved. The wedging eliminated far-infrared interference fringes from the sample. The surface was not treated in any special way since only bulk absorption was investigated.

Spectra were measured with a Research and Industrial Instruments Co. model FS-720 far-infrared Michelson interferometer covering the frequency range 0–625 cm^{-1}. A gallium-doped germanium bolometer detector was designed and constructed for pumped-helium temperatures to benefit from low-temperature operation. The noise-equivalent power of the detector was about 6×10^{-13} W/Hz$^{1/2}$. The bolometer signal received an initial power gain of about 10^8 in a preamplifier which was a modified version of a design by Zwerdling *et al.*[8] It featured high-input impedance for proper matching to the bolometer's resistance and an output impedance of 1 Ω. The preamplifier output was coupled to the input stage of a lock-in amplifier through a 100-to-1 step-up transformer. The output of the lock-in amplifier was continuously monitored with a strip-chart recorder and digitized by a voltmeter capable of a resolution of 1 part in 10^5. The parallel binary-coded decimal (BCD) output from the voltmeter was sequentially fed to an incremental magnetic-tape recorder through a serializer.

The spectrum was obtained by performing a Fourier transform of the interferogram stored on the magnetic tape. The computer program apodized the interferogram using a triangular function and then corrected for zero-path-difference errors using a procedure due to Forman *et al.*[9] Typically, 6250 interferogram points were transformed using the fast-Fourier-transform algorithm to produce a spectrum with 0.2-cm^{-1} resolution.

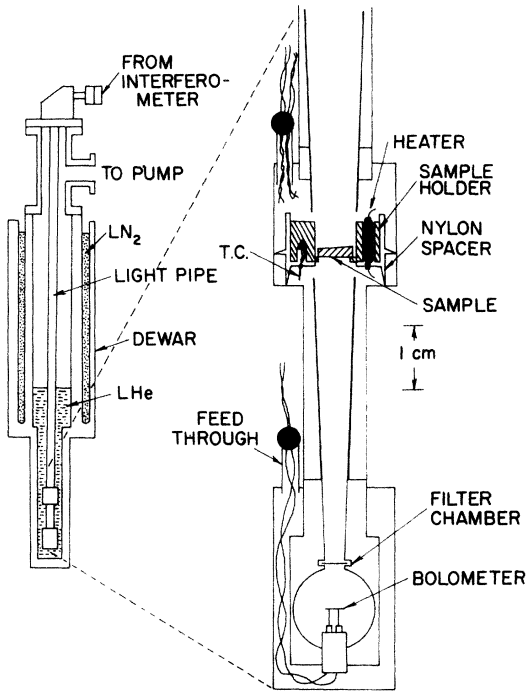

FIG. 1. Schematic cross-sectional view of sample assembly.

A schematic cross-sectional view of the sample assembly is shown in Fig. 1. It was designed to permit transmission spectra of a sample to be taken as a function of temperature. The assembly was situated in a stainless-steel Dewar containing a pumped-helium bath which kept the detector at its operating temperature of 2 K. Provision was made to increase the temperature of the sample without seriously affecting the operation of the bolometer located 5.5 cm below it.

Light reached the sample chamber after proceeding through about 1 m of 1.3-cm-i.d. polished-brass light pipe. A long condensing cone reduced the aperture above the sample chamber. The sample holder was a copper cylinder with a 6-mm-diam hole in the center. The sample was seated on a lip in this hole held in place with silver paste. Two holes, 180° apart, were drilled in the sample holder to accommodate a heater, which was a $\frac{1}{8}$-W carbon resistor, and a copper-constantan thermocouple. The copper sample holder was thermally insulated from the walls by a nylon spacer. Utilizing a negative-feed-back system, the temperature of the thermocouple was stabilized to within

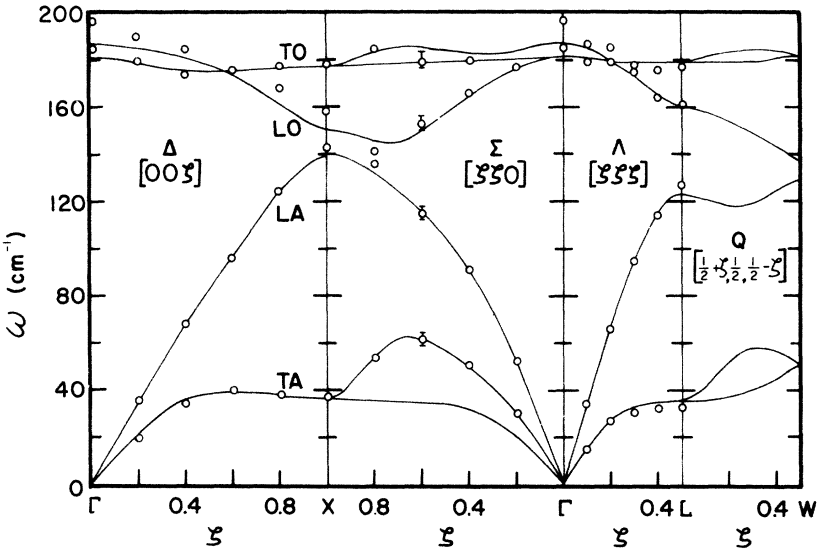

FIG. 2. Phonon-dispersion curves in InSb. The circles are the values determined by Price *et al.* (1971) at 300°K by inelastic neutron scattering. The dispersion curves were measured in the $\Delta([00\zeta])$, $\Sigma([\zeta\zeta 0])$ and $\Lambda([\zeta\zeta\zeta])$ symmetry directions. The solid lines are the calculated dispersion curves in the Δ, Σ, Λ and Q [along the (111) plane from L to W] directions. The curves are labeled according to their vibrational nature near X in the Δ direction; TA (transverse acoustic), LA (longitudinal acoustic), LO (longitudinal optic), and TO (transverse optic).

1 K. After traversing the sample, the light passed through another condensing cone and a filter chamber before entering a 1.3-cm-diam integrating sphere which contained the detector.

III. RESULTS

A. Single-phonon absorption

Single-phonon absorption was studied in a thin wedge-shaped sample, with a thickness varying between 0 and 75 μm from side to side. The Reststrahl absorption involving the TO-phonon mode at Γ was centered at 186 cm^{-1}. A second absorption peak observed at 198.6 cm^{-1}, which was sharp and intense relative to absorption from two-phonon processes, was considered to involve the LO phonon at Γ. For the observation of this mode, the face of the sample was not normal to the incident light and the sample was thin enough over most of its area so that the criteria of Berreman[10] for longitudinal-optical-phonon absorption, which requires oblique incidence of infrared radiation on a sample with a thickness comparable to optical-phonon wavelengths, were fulfilled. The temperature dependence of this absorption was typical of single phonons: As the temperature increased it broadened slightly but did not increase in intensity. Strong two-phonon absorption was not expected at this frequency according to the calculated density-of-states curve.

B. Two-phonon absorption

The absorption strength of the two-phonon spectrum is a product of three terms: the thermal-phonon population, the magnitude of the photon-phonon coupling mechanism, and the density of two-phonon states. The first term is readily calculable employing Bose-Einstein distribution functions. Its main consequences are that two-phonon difference modes are absent at low temperature but increase rapidly in strength with increasing temperature. Two-phonon sum modes are present even at zero temperature but are less dependent upon temperature.

Van Hove[2] has shown that critical points on phonon-dispersion curves lead to particular types of discontinuities on the density-of-states curves. The dispersion curves of InSb as measured by Price *et al.*[5] are presented in Fig. 2. A critical point is a location in the Brillouin zone at which the phonon energy is constant or a weak function of wave vector. The exact shape of the resultant discontinuity is dependent upon whether the phonon-dispersion curve $\omega(\vec{k})$ at some critical point, defined by $\nabla\omega(\vec{k}) = 0$, is a minimum in three, two, one, or no principal directions. These situations correspond to a three-dimensional minimum, two kinds of saddle points, and a three-dimensional maximum and produce the discontinuities in the density of states, labeled P_0, P_1, P_2, and P_3, respectively, illustrated in Fig. 3. Using group theory, Phillips[11] has extended van Hove's work to show that the minimum set of such critical points must include the high-symmetry points in the Brillouin zone. The locations of these points on the Brillouin zone of InSb [$\Gamma(0, 0, 0)$, $X(1, 0, 0)$, $L(\frac{1}{2}, \frac{1}{2}, \frac{1}{2})$ and $W(1, \frac{1}{2}, 0)$] are pictured in Fig. 3. Other critical points at off-symmetry-axes positions are also possible but their exact locations must be found in a more empirical fashion. With a knowledge of the phonon energies throughout the whole Brillouin zone, for all branches, the posi-

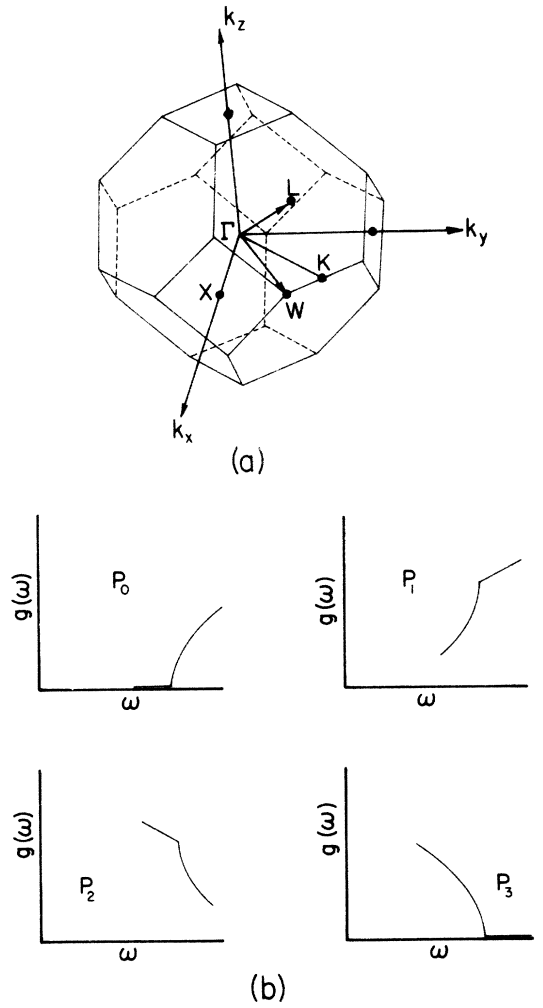

FIG. 3. (a) Brillouin zone of InSb. (b) Discontinuities in the phonon density of states produced by four types of critical points on dispersion curves: P_3, a point of maximum phonon energy; P_0, a point of minimum phonon energy; P_2, a saddle point with energy increasing in one principal direction; P_1, a saddle point with energy increasing in two principal directions.

tion of important critical points can be discovered using phonon-energy-contour analysis. Thus calculated phonon energies for a given combination of branches were plotted as a function of wave-vector components on certain symmetry planes. Contours of constant two-phonon energy were drawn as illustrated in Fig. 4. The positions and types of critical points present were derived by locating areas in which the energy was a maximum, a minimum, or exhibited saddle-point behavior. In this manner information concerning the critical points of 21 two-phonon sum modes on the (100), (111), and (110) symmetry planes was obtained. Then, those critical points giving rise to prominent features on the calculated two-phonon density of states were identified.

The phonon energies employed in the energy-contour analysis and used to derive the two-phonon density-of-states curves were calculated using parameters derived from inelastic-neutron-scattering experiments.[5] This calculation, based on a shell model with second-neighbor short-range forces, is similar to one used previously on GaAs by Dolling and Cowley.[12] The secular lattice equation was solved at 874 uniformly distributed points in the irreducible part of the first Brillouin zone. An interpolation scheme was then employed to

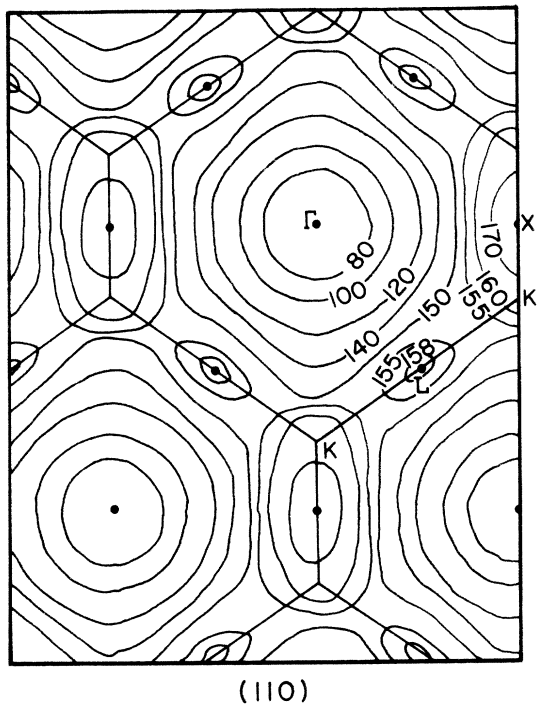

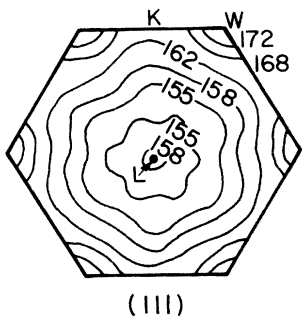

FIG. 4. Contours of constant energy (in cm^{-1}) for the LA + TA_2 phonon combination on the (111) and (110) planes. The (110) plane is pictured in the extended zone scheme. Areas of maximum energy are located at X, L, and W.

derive extra values for phonon energies between the points. A total of about 1.4×10^8 frequencies for all the phonon branches throughout the whole zone were obtained. The single-phonon density of states was determined in a straightforward manner by counting the total number of frequencies present in each frequency interval of 0.33 cm^{-1}. The second-harmonic density-of-states spectrum was identical to the first with the frequency scale doubled. The other two-phonon density-of-states curves were derived using the same procedure for combinations formed by adding or subtracting the frequencies of phonons from different branches but possessing the same wave vector. This latter requirement is a consequence of momentum conservation. No selection rules were applied in these calculations.

The identification of the structure on the absorption spectra was accomplished by comparing them with the calculated two-phonon density-of-states curves. A one-to-one correspondence between the two curves could be found for most of the features. These features were then correlated with specific two-phonon combinations at particular critical points using the results of the phonon-energy-contour analysis. However, there were some discrepancies and so, as an added check, experimental two-phonon dispersion curves were formed by combining measured phonon branches in symmetry directions. Critical points along dispersion curves appear as maxima or minima but their exact three-dimensional nature cannot be discerned without information about off-axis phonon energies. All of the remaining prominent peaks in the absorption curves were identified utilizing these empirical two-phonon-dispersion curves. They were found to involve phonons combining with the transverse optic mode which the shell-model calculation has a tendency to flatten. This effect leads to a narrowing of optic overtone peaks and peaks involving optic modes in the density of states and thus to a loss of structure.

There are several features that are reported which were difficult to assign unambiguously due to their small amplitudes. Their positions are included for completeness. Also taken into account in the assignments was the fact that the experimental dispersion curves were measured at room temperature where the phonon frequencies are slightly lower (about 1–2%) than at the low temperatures employed in this experiment.

1. Sum combinations

In Fig. 5 the observed absorption of two-phonon sum modes from 60 to 380 cm^{-1} at 20 K is compared with the density-of-states calculation for two-phonon sum modes. Thick samples were necessary in order to observe adequate two-phonon absorption. The strong Reststrahl band dominates the two-phonon absorption in the region around 186 cm^{-1}. The experimental spectra studied were the average of two or more runs with the instrumental background removed by ratioing with spectra obtained with no sample in the beam. The assignment of spectral features to critical points of two-phonon sum modes is summarized in Table I. For convenience, the phonons are labeled TO_1, TO_2, LO, LA, TA_1, and TA_2 in the order of decreasing frequency near X even though it is strictly correct to speak of pure transverse or longitudinal modes of vibration only in certain symmetry directions. The shapes of the spectral discontinuities, as set down in Table I, were derived from phonon-energy-contour analysis and, in all

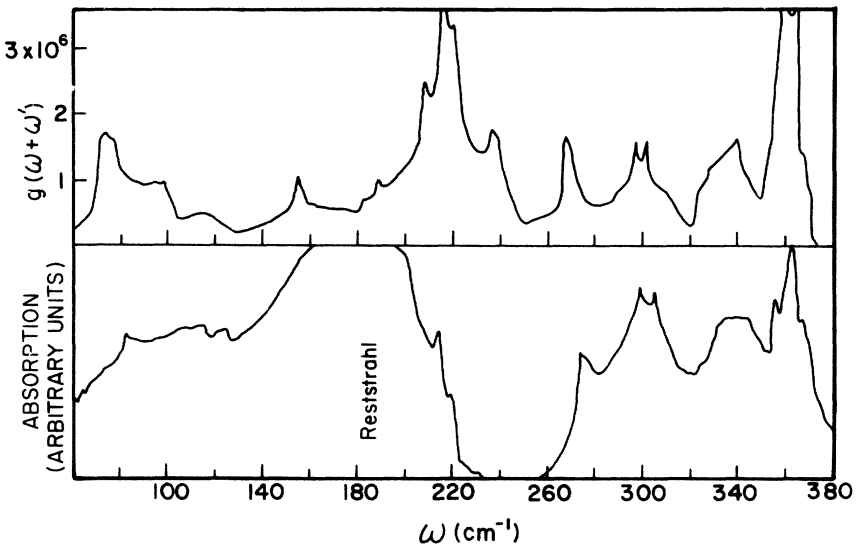

FIG. 5. Comparison of the calculated two-phonon density of states for summation processes with the observed absorption in the frequency range 60–380 cm^{-1} with a sample temperature of 20 °K. The sample thickness was 1800 μm in the regions 60–200 cm^{-1} and 250–380 cm^{-1} and was 250 μm from 200 to 250 cm^{-1}.

TABLE I. Two-phonon sum modes.

Experimental Feature			Assignment Critical Points: Energy Contour Analysis		Experimental Dispersion Curves
Position (cm^{-1})	Strength	Combination	Location	Shape	Location
82.6	medium	2TA	(0.6, 0, 0)	P_1+P_2	(0.6, 0, 0)
84–87	weak				
115	medium	TA_1+TA_2	K	P_2	
117	medium	TA_1+TA_2	W	P_3	
124	medium	$2TA_1$	hexagonal face	P_2	
127	medium	$2TA_1$	(0.6, 0.6, 0)	P_3	(0.6, 0.6, 0)
161	medium	$LA+TA_2$	hexagonal face	P_1+P_2	
208.1	medium	$LO+TA_1$	(0.25, 0.25, 0.25) and hexagonal face	P_1+P_2	(0.25, 0.25, 0.25)
211.2	very weak				
213.5	strong	TO+TA	X	P_1+P_2	L
214.4	strong	LO+TA	near K and (0.25, 0.25, 0.25)	P_1+P_2	(0.2, 0.2, 0.2)
218.6	strong	Optic+TA	(0.6, 0, 0)	P_1+P_2	(0.6, 0, 0)
220.0	strong	TO+TA	L	P_1+P_2	X
225	weak	TO_1, $LO+TA_1$			(0.4, 0, 0), (0.5, 0.5, 0)
240	very weak	$TO_{1,2}+TA_1$	near K and W	P_1+P_3	K
246.2	weak	2LA	hexagonal face	P_1+P_2	
273.2	very strong	LO+LA	hexagonal face	P_1	
273.2	strong	LO+LA	near W	P_2	
277.6	medium	LO+LA	near K	P_2	
298.8	strong	TO_2+LA	hexagonal face	P_1+P_2	
305	strong	TO_1+LA	hexagonal face	P_1+P_2	
320	weak				
322	weak				
326	medium	$TO_{1,2}+LO$	W	P_0	
344.8	medium	TO+LO	L	P_2	X, L
349	weak	2TO			(0.4, 0, 0)
355.5	strong	Optic overtone			(0.6, 0, 0)
358.9	medium	2TO	X		L
362.7	strong	2TO	hexagonal face and L	$P_1+P_2+P_3$	X
367	medium	TO_1+TO_2, LO	W	P_1+P_2	
370	weak	2TO	W and hexagonal face	P_1+P_2	
375	weak				
384–388	weak				

cases, are confirmed by the observed structure.

At frequencies less than the Reststrahl band, the two-phonon sum bands are primarily due to combinations of acoustical modes; $2TA_1$, $2TA_2$, TA_1+TA_2, 2LA, $LA+TA_1$, and $LA+TA_2$. The agreement between the density-of-states calculation and the experimental spectrum is less satisfactory in this region than in any other part of the spectrum although the over-all shapes of the two curves are similar. This is surprising in view of the fact that the fit of the calculated dispersion curves to the experimental curves for the acoustic modes in the symmetry direction is good as shown in Fig. 2. The frequencies of the observed features, with the exception of the sudden decrease in absorption at 127 cm^{-1} which is attributed to a maximum in the $2TA_1$ branch at (0.6, 0.6, 0), are higher than similar features on the calculated curve. However, using the two-phonon density-of-states curve and the results of energy-contour analysis, the peak at 124 cm^{-1} can be attributed to a $2TA_1$ overtone mode at a critical point halfway between L and W on the hexagonal face (111) plane of the Brillouin zone. Similarly, the shoulder that occurs at 115 cm^{-1} is due to a critical point on the TA_1+TA_2 combination branch near K(0.75, 0.75, 0) and the cut-off that takes place at 117 cm^{-1} is ascribed to a critical point in the same branch at W.

Absorption due to critical points on the 2TA branch at X and L which is expected at 68–78 cm^{-1}

from the density-of-states calculation is not observed. Just outside this frequency region, a small but extremely sharp peak at 82.6 cm^{-1} is present with a broad weak shoulder on the high-energy side of this peak and a weaker peak on the low-energy side. From the experimental dispersion curves it is evident that the sharp peak must be related to the maximum at (0.6, 0, 0), on the degenerate transverse-acoustic branches. The energy-contour analysis confirms this assignment and elucidates the formation of this feature. One of the two degenerate TA modes at this point contributes a type-P_1 discontinuity to the density-of-states curve while the other results in a discontinuity of type-P_2. The sum of these produces a weak cusp in the density-of-states at 79 cm^{-1}. The absence of strong absorption attributable to critical points at X and/or L on the 2TA branch is unexpected in that, the TA dispersion curves are relatively flat at and near these points, the density-of-states calculation possesses a large peak, and the selection rules do not forbid it. A similar situation has been reported in GaAs,[13] and confirmed by us in preliminary studies. Again there is a strong broad peak predicted by the density-of-states calculation due to critical points at X and L on the 2TA branches but only a weak relatively sharp absorption is observed in the spectrum. These results emphasize the importance of accurate calculations of the appropriate matrix element for obtaining the strength of the infrared absorption.

Most of the features due to critical points on the LA + TA branches were expected at frequencies such that they would be hidden by the strong Reststrahl absorption. However, a relatively strong, narrow line due to critical points on the LA + TA_2 branch was observed at 161 cm^{-1} on the edge of the strong absorption band. This sharp cusp-shaped peak results from P_1- and P_2-type critical points on the hexagonal face of the Brillouin zone. The constant energy contours for the LA + TA_2 branch on the (111) and (110) symmetry planes are illustrated in Fig. 4. The most interesting feature on the hexagonal face (111) is an approximately circular valley centered on the L point which results from points with approximately the same energy but with differing wave vectors. From a consideration of Fig. 4 it is evident that moving away from this valley towards L, K, or W in the (111) plane results in an increase in phonon energy while moving at right angles to this plane towards the center of the Brillouin zone at Γ produces a decrease in energy. Thus, the valley appears to be composed of critical points of the saddle-point type. As one proceeds along this valley a move upward in energy indicates a saddle point of type P_1 while a decrease in energy identifies a P_2-type critical point. These have approximately the same energy and so a cusplike peak is formed at 161 cm^{-1}.

On the immediate-high-energy side of the Reststrahl band are features produced by critical points on the transverse acoustical plus optical sum branches. The prominent structure results from critical points which occur at high-symmetry points or along symmetry axes where the transverse modes are degenerate. Thus, it is possible to speak principally of TO + TA modes. Generally, the assignments as given by the energy-contour analysis agree with those deduced from a study of the experimental two-phonon dispersion curves. However, when there are discrepancies, as in the position of features ascribed to the X and L points, greater reliance is placed on the analysis based on the experimental dispersion curves for reasons mentioned previously. The strongest peaks, visible even in thin samples, occur at 213.5 and 218.6 cm^{-1} and are due to critical points on the TO + TA branch at the L point and (0.6, 0, 0), respectively. There are shoulders present on both of these peaks due to critical points on optic + TA branches. The critical points that produce the features at 214.4 and 220.0 cm^{-1} occur at (0.2, 0.2, 0.2) and X, respectively. Other weaker features occur at 225 and 240 cm^{-1}. Also contributing is a weak peak at 246.2 cm^{-1} due to P_1 and P_2 critical points on the (111) plane of the LA overtone branch. The situation resulting in the narrow peak is similar to the one described above for the LA + TA_2 branch.

The features due to critical points on the LO + LA, TO_1 + LA, and TO_2 + LA branches occur in the region from 250 to 320 cm^{-1}. The LA-phonon mode, whose energy is a strong function of wave vector, imposes its behavior near the zone boundary on the weakly varying optic modes to produce the sharp peak visible at 273.2 cm^{-1} and the narrow twin peaks centered on 300 cm^{-1}. A study of the energy contours on the (111) plane of the TO_1 + LA and TO_2 + LA branches reveals a situation analogous to that for the LA + TA_2 mode. The transverse-optic modes are not degenerate on the (111) plane and so two peaks, equally sharp, are produced. In the case of the LO + LA branch, a large volume of k space near the zone boundary is found to be relatively stable in energy. But it again appears that the dominant critical points occur at or near the hexagonal face although the over-all shape of the peak is the result of an averaging process over a large volume in this region of k space.

Combinations of TO and LO modes produce infrared-absorption bands at frequencies ranging from 320 to 400 cm^{-1}. The discrepancy between experiment and the density-of-states curve expected in this region because of the flattening of

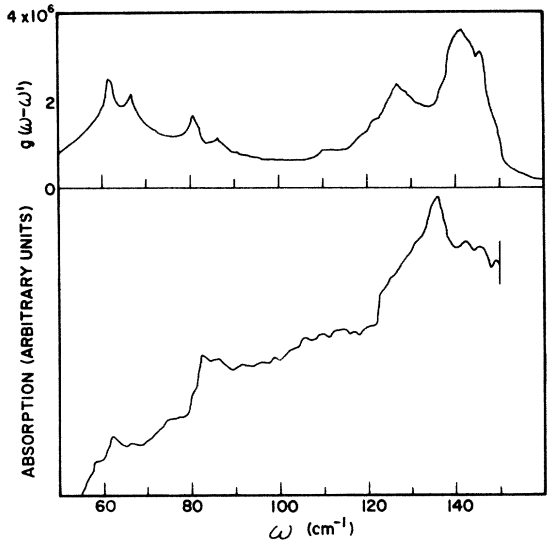

FIG. 6. Calculated density of states for two-phonon difference processes compared with the observed absorption in an 1800-μm-thick sample at 78 °K in the frequency range 50–160 cm^{-1}.

the optical modes in the calculation is less serious than feared. The principal difference appears to be the absence, in the calculated density of states, of a strong subsidiary peak, at 355.5 cm^{-1}, of the main peak at 362.7 cm^{-1}. The broad mesa-shaped absorption extending from about 330 to 345 cm^{-1} is the result of combinations of LO and TO modes at various locations throughout the zone. The cutoff in absorption at 344.8 cm^{-1} is due to a P_2 critical point at L according to energy-contour analysis. Overtones of TO branches produce the absorption that begins at 350 cm^{-1}. According to energy-contour analysis many of the features in this region can be attributed to critical points on the hexagonal face for the TO overtone modes. However, the over-all picture is complicated and some doubts exist as to its validity because of the problem related to the flattening of the optical modes by the calculation. Thus more reliance is placed on the identifications based on the analysis of the experimental dispersion curves. In this case the main peak at 362.7 cm^{-1} is attributed to critical points at X, the low-energy shoulder, which is noticeable as an asymmetry of the main peak, to critical points at L, and the subsidiary peak at 355.5 cm^{-1} to critical points at (0.6, 0, 0). All of these occur on the 2TO branch. A number of other weaker features are present at higher frequencies but are difficult to assign unambiguously.

2. *Difference combinations*

The experimental details relating to the two-phonon difference spectrum are similar to those outlined for the two-phonon sum spectrum. The only variation was the utilization of the rapid increase of absorption with temperature, characteristic of two-phonon difference bands, to distinguish them from sum bands which are present in the same region of the spectrum. A spectrum taken with a sample temperature of 78 °K in which the difference bands were quite strong was ratioed with one at 20 °K in which they were essentially absent. This procedure accentuated the difference bands although the sum bands were not completely cancelled because they do possess some temperature dependence.

The experimental absorption spectrum and the calculated density of states for two-phonon difference modes are presented in Fig. 6. The assignment of the modes is given in Table II. The principal feature, a strong relatively sharp peak at 136 cm^{-1}, results from critical points at (0.6, 0, 0) on the TO – TA branch. Although such a feature is

TABLE II. Two-phonon difference modes.

Experimental feature			Assignment critical points Energy-contour analysis		Experimental dispersion curves
Position (cm^{-1})	Strength	Combination	Location	Shape	
61.5	weak	LA – TA$_1$	hexagonal face	P_1+P_2	
73–78	weak				
80–82	weak	LA – TA$_2$	hexagonal face	P_1+P_2	
86	weak	LO – TA$_1$	K	P_0+P_2	K
122	medium	TO$_{1,2}$ – TA$_1$	K	P_0	(0.6, 0.6, 0)
127	medium	TO – TA	hexagonal face	P_1+P_2	
136	strong	Optic – TA	(0.6, 0, 0)	P_0+P_2	(0.6, 0, 0)
142.5	weak	TO – TA	X	P_1+P_2	X
146	weak	TO – TA	L	P_1+P_2	L

predicted by energy-contour analysis the observed strength is not. The weak subsidiary peaks on the high-energy side of the 136-cm^{-1} absorption are due to critical points on the TO – TA branch at X(142.5 cm^{-1}) and L(146 cm^{-1}), respectively. These are predicted although in the calculated density of states they are merged into one broad peak centered on 141.5 cm^{-1}. According to energy-contour analysis, a number of critical points on the TO – TA branch on or near the hexagonal face produce the peak present at 127 cm^{-1} in the density-of-states curve. This is observed as a low-energy shoulder on the 136-cm^{-1} peak.

At much lower energies a sharp peak is present at 61.5 cm^{-1} in the absorption spectrum. This can be correlated with critical points on the hexagonal face for the $TO_2 - LA$ and $LA - TA_1$ branches. Due to the influence of the LA mode there is a low circular mound consisting of P_1- and P_2-type critical points degenerate in energy present on the (111) plane for these difference branches. A similar mound for the $TO_1 - LA$ branch produces a sharp peak in the difference density of states at 66.8 cm^{-1}. This is not observed experimentally. However, if the assignment of the 2LA mode on the (111) plane is correct, then, using the known values of critical points of $TO_1 + LA$ and $TO_2 + LA$ on the hexagonal face, the values of $TO_1 - LA$ and $TO_2 - LA$ become 59 and 53 cm^{-1}, respectively, in this area. The situation could be clarified by inelastic-neutron-scattering experiments performed in the Q direction.

Finally the energy-contour analysis predicts relatively sharp but weak peaks near 81 and 86 cm^{-1} resulting from critical points on the $LA - TA_2$ branch and the $LO - TA_1$ branch respectively. This is in the region in which the sharp peak due to critical points at (0.6, 0, 0) on the 2TA branch occurs and so these difference bands are difficult to observe clearly. However, judging from the temperature dependence of the absorption in this region, it is likely that difference bands do underlie the prominent summation absorption.

IV. DISCUSSION

The over-all shapes, positions, and intensities of features of the two-phonon absorption spectra of InSb correlate well with calculated two-phonon density-of-states curves. The analyses of phonon-energy contours on symmetry planes and experimental two-phonon dispersion curves indicate that most prominent features of the spectrum can be attributed to critical points in the Brillouin zone at (0.6, 0, 0), X, and L for phonon combinations involving transverse modes and on the hexagonal face, the (111) plane, for combinations containing the longitudinal acoustical phonon. This latter observation confirms Borik's comment[14] in a theoretical paper on the significance of the hexagonal face for the distribution of combined phonon frequencies in GaAs. This is a III-V compound semiconductor with dispersion curves and a two-phonon absorption spectrum similar to that of InSb.

At X and L, phonon combinations possessing critical points which lead to prominent features in the calculated spectrum include 2TA, TO + TA, 2TO, and TO – TA. Critical points of transverse-phonon-mode combinations at (0.6, 0, 0) also figure prominently in the observed spectrum. This is an interesting location in the Brillouin zone as it is the point in the [100] direction at which the transverse- and longitudinal-optic modes are degenerate and the degenerate transverse-acoustic branches exhibit a maximum. Thus it is not entirely surprising that this position in the Brillouin zone produces so many prominent features in the two-phonon spectrum [at 82.6 cm^{-1} (2TA), 218.6 cm^{-1} (optic + TA), 355.5 cm^{-1} (optic overtone), and 136 cm^{-1} (optic – TA)]. The absence of the features containing the optic mode in the two-phonon density-of-states calculations apparently arises because of the inadequate treatment of the optical-phonon modes by the shell-model theory. For this reason, in the analysis of critical points of phonon combinations involving optical modes more reliance was placed on the identification provided by studying the experimental dispersion curves than on the energy-contour analysis.

Ironically, early work on the interpretation of the multiphonon spectra of InSb appears to be more nearly correct than later, more detailed, analyses. Fray *et al.*[3] first correlated spectral features with combination bands involving four-phonon frequencies which were described as averages over the Brillouin-zone boundary where phonon energies were expected to be relatively stable. This relatively crude picture agreed rather well with the detailed analysis presented here. Later, attempts[4,5] were made to identify the fine structure of the spectrum with critical points of phonon-mode combinations at the high-symmetry points X and L without the benefit of experimental dispersion curves. These were much less successful, as is evident in Table III.

Utilizing the frequencies of combination modes from critical points at X, L, and (0.6, 0, 0), explicit phonon frequencies for some modes at these points were derived. These are presented in Table IV along with the results of Price *et al.*[5] (inelastic neutron scattering), Johnson[1] (infrared absorption), and Stierwalt[4] (infrared emission). The agreement between the values derived from this work and those measured directly by inelastic neutron scattering is good, especially when allowance is made for the temperature shift of the phonon frequencies.

TABLE III. Comparison of two-phonon assignments by various workers.

Previous work			This work	
Position of feature (cm^{-1})	Assignment		Position of feature (cm^{-1})	Assignments
	Johnson	Stierwalt		
83		2TA(*X*)	82.6	2TA(0.6, 0, 0)
98		TO(Γ) − 2TA(*X*)	115	$TA_1(K) + TA_2(K)$
111		2TA(*L*) + TA(*X*)	117	$TA_1(W) + TA_2(K)$
124		3TA(*X*)	124	$2TA_1$ (hexagonal face)
			127	$2TA_1$ (0.6, 0.6, 0)
136	TO(*L*) − TA(*L*)	TO(*L*) − TA(*L*)	136	Optic (0.6, 0, 0) − TA (0.6, 0, 0)
159		LA(*W*) + TA(*W*)	161	LA + TA_2 (hexagonal face)
205		2LA(*L*)		...
		TO(*L*) + TA(*L*)	208.1	LO (0.25, 0.25, 0.25) + TA_1 (0.25, 0.25, 0.25)
			213.5	TO(*L*) + TA(*L*)
			214.4	LO (0.2, 0.2, 0.2) + TA (0.2, 0.2, 0.2)
			218.6	Optic (0.6, 0, 0) + TA (0.6, 0, 0)
			220	TO(*X*) + TA(*X*)
			246.2	2LA (hexagonal face)
273	2LA(*L*)		273.2	LO + LA (hexagonal face)
297	LO(*L*) + LA(*L*)		298.8	TO_2 + LA (hexagonal face)
302	LO(*X*) + LA(*X*)		305	TO_1 + LA (hexagonal face)
337	TO(*X*) + LO(*X*)		344.8	TO(*L*) + LO(*L*) TO(*X*) + LO(*X*)
353	2TO(*X*)		355.5	Optic (0.6, 0, 0) overtone
			358.9	2TO(*L*)
361	2LO(*L*)		362.7	2TO(*X*)
400	LO(Γ) + TO(Γ)			
412	2LO(Γ)			

Finally, it should be mentioned that the over-all shapes of two-phonon absorption spectra of other III-V compound semiconductors (such as GaAs and InAs) bear a striking resemblance to that of InSb. It should be possible, using the analyzed InSb spectrum as a guide, to identify major features in

TABLE IV. Comparison of frequencies of phonon modes at *X*, *L*, and (0.6, 0, 0) determined by various workers (cm^{-1}).

Location	Phonon mode	Price *et al.* (300°K)	This work (20°K)	Johnston [(4.2–90)°K]	Stierwalt [(4.2–77)°K]
Γ	TO	185 ± 2	186	189.5	182
(0, 0, 0)	LO	197 ± 8	198.6 ± 0.1	205.7	195
	TO	179.5 ± 5.7	181.4 ± 0.2	176.6	176
X	LO	158.4 ± 6.7	163.4 ± 0.2	159.7	129
(1, 0, 0)	LA	143.4 ± 3.3		142.8	121
	TA	37.4 ± 1.7	38.6 ± 0.2		41.5
	TO	177.1 ± 2.0	179.8 ± 0.2	179.9	171
L	LO	160.8 ± 3.3	165.0 ± 0.2	160.5	160
(0.5, 0.5, 0.5)	LA	127.1 ± 2.0		136.3	102
	TA	32.7 ± 1.7	33.8 ± 0.2	43.6	34
(0.6, 0, 0)	TO	176.1 ± 2.7	177.7 ± 0.5		
	TA	40.0 ± 1.3	41.3 ± 0.1		

the spectra of these materials with some confidence, even in the absence of experimental dispersion curves.

V. CONCLUSIONS

Most of the prominent features present on high-resolution two-phonon absorption spectra of InSb correlated with structure on two-phonon density-of-states curves calculated in an independent manner using parameters derived from inelastic-neutron-scattering experiments. The agreement makes possible a detailed energy-contour analysis of all two-phonon branches on certain symmetry planes in order to locate the critical points responsible for the observed features. Critical points at off-symmetry axes locations on or near the Brillouin-zone boundary produce much of the prominent structure. Thus in the critical-point analysis of multiphonon spectra such "accidental critical points" cannot be ignored as has been generally done. The derived phonon energies at certain points in the Brillouin zone are given in Table IV. The 2TA overtones at X and L are not observed. This shows that the density-of-states curves does not completely explain the infrared absorption and that the matrix elements for the strength of the infrared absorption should be calculated.

ACKNOWLEDGMENTS

The authors have benefited from the cooperation on far-infrared techniques with Dr. Timusk and members of his research group. Thanks are extended to Dr. Timusk for suggestions about energy contour analysis, to R. Douglas for his work on the far-infrared spectrometer, and to C. Verge for constructing the electronics of the spectrometer.

---

†Research supported in part by the National Research Council of Canada.

[1]F. A. Johnson, Prog. Semicond. 9, 179 (1965).
[2]L. van Hove, Phys. Rev. 89, 1189 (1953).
[3]S. Fray, F. A. Johnson, and R. Jones, Proc. Phys. Soc. Lond. 76, 939 (1960).
[4]D. Stierwalt, J. Phys. Soc. Jap. Suppl. 21, 58 (1966).
[5]D. Price, J. Rowe and R. Nicklow, Phys. Rev. B 3, 1268 (1971).
[6]B. Szigeti, Proc. R. Soc. Lond. A 252, 217 (1959); 258, 377 (1960).
[7]R. Geick, Phys. Rev. 138, A1495 (1965).
[8]S. Zwerdling, J. P. Thereault, and H. S. Richards, Infrared Phys. 8, 135 (1968).
[9]M. J. Forman, W. H. Steel, and G. A. Vanasse, J. Opt. Soc. Am. 56, 59 (1966).
[10]D. Berreman, Phys. Rev. 130, 2193 (1963).
[11]J. Phillips, Phys. Rev. 104, 1263 (1956).
[12]G. Dolling and R. Cowley, Proc. Phys. Soc. Lond. 88, 463 (1966).
[13]R. Stolen, Appl. Phys. Lett. 15, 74 (1969).
[14]H. Borik, Phys. Status Solidi 39, 145 (1970).